Adaptive Sliding Mode Control of Parallel Sorting Robots Using Variable-Gain Super-Twisting ESO

Luqing Guo

Department of Network Security, Henan Police College, Zhengzhou 450046, China

Email: glq_haohao666@163.com

Keywords: ESO, adaptive control, sorting parallel robot, control system

Received: April 11, 2025

Parallel robots have uncertain problems such as time-varying model parameters and external disturbances. When the sorting load is unknown and changes dynamically, the load moment of inertia will change significantly when the sorting objects are connected in series. This paper proposes a sorting parallel robot control system that combines ESO and adaptive control, thereby improving the control effect of the sorting parallel robot and improving the control efficiency of the parallel robot. The new controller (IM-ST-ESO) is based on OLI-SMC and IASMC. And designs an adaptive law to weaken the dependence of the generalized super-twisting sliding mode algorithm on the disturbance boundary, improve the anti-disturbance ability of the system, and further improve the convergence speed of the system through the linear terms in the integral fast non-singular sliding surface. Combined with the experimental analysis, The experimental method has achieved significant results in optimizing the running time of the Delta robot sorting process. After optimization, the running time is 0.231s, which is 6.60% lower than before optimization. The average impact of each joint of the driving arm is significantly reduced, and the impact is reduced by 80.00%. Reducing joint impact helps improve the operational efficiency of robots and extend their lifespan. At the same time, it significantly reduces the average impact of each joint of the drive arm, and the impact is reduced by 80.00%. Therefore, it can be seen that the sorting parallel robot control system combined with ESO and adaptive control can effectively improve sorting efficiency and system performance, and can play an important role in subsequent intelligent production and intelligent operation.

Povzetek: Članek predstavi IM-ST-ESO: adaptivno drsno vodenje robota s super-twisting ESO s spremenljivim ojačanjem in hiperbolično zamenjavo signuma, kar zmanjša trepetanje, pospeši konvergenco ter izboljša sledenje in robustnost.

1 Introduction

Trajectory tracking, as one of the key technologies of parallel robots, can accurately run along the predetermined trajectory and has become a hot topic in current research.

The application of parallel robot in industry mainly focuses on precise positioning and ideal dynamic characteristics, so dynamic analysis is necessary. Common position-based kinematics feedback control method is difficult to have accurate control accuracy and response speed. Moreover, PID feedback control is a common control scheme in industry. When using this scheme for trajectory planning, the limitation of robot power system cannot be reasonably considered, and the speed or acceleration trajectory exceeds the physical limitation of motor can be generated.

The traditional Delta parallel robot controls the end of the robot to complete the corresponding tasks according to the planned path through teaching programming, accuracy and stability. When the working conditions change, it is necessary to re-program the parallel robot according to the actual working conditions to meet the new working requirements. Therefore, the traditional Delta parallel robot does not have the flexibility to adapt to changeable working tasks, and is only suitable for a single task and a relatively fixed working environment. With the optimization and upgrading of the industrial structure of manufacturing industry, Delta parallel robots based on teaching programming are difficult to meet the needs of flexible manufacturing on intelligent production lines. Therefore, on the basis of traditional teaching programming, vision sensors are gradually applied to Delta robots. As the "eyes" of robots, visual sensors enhance the robot's ability to perceive the surrounding environment, enabling the robot to analyze, process and judge the surrounding environment, and guide the robot to complete complex and diverse tasks [1]. Applying visual sensors to industrial robots and guiding and controlling them belongs to the application scope of machine vision. Industrial robots equipped with machine vision have the advantages of accurate positioning, high operating efficiency and high flexibility. In addition, they can use machine vision to recognize, classify and determine the

position and posture of workpieces, thereby planning trajectories to guide the robot to perform actions to complete corresponding work tasks, which greatly improves the robot's work efficiency [2]. Nowadays, the manufacturing cost is increasing day by day, the speed of product iterative upgrading is accelerating, and new products are constantly being launched. Therefore, the intelligent transformation of industrial production lines is urgent [3]. Based on the urgent demand of visually guided Delta parallel robot in industrial automation production line, this paper not only improves the accuracy of visual recognition and positioning, but also ensures the reliability of real-time tracking of moving workpieces, and provides accurate workpiece category and position information for subsequent Delta robot to perform sorting tasks, which has important theoretical value and practical significance to improve the intelligent level of Delta parallel robot.

This work proposes a variable-gain ST-ESO based control architecture for parallel Delta robots to improve sorting accuracy, robustness, and computation efficiency under variable load conditions. This paper proposes a sorting parallel robot control system that combines ESO and adaptive control, thereby improving the control effect of the sorting parallel robot and improving the control efficiency of the parallel robot. Moreover, this paper uses a hyperbolic function to replace the sign function in the super-twisting sliding mode expansion state observer to further reduce system chattering. In addition, this paper designs a variable gain function that can change in real time with the observation error to replace the linear gain of ST-ESO, and designs an adaptive law to weaken the dependence of the generalized super-twisting sliding mode algorithm on the disturbance boundary, improve the anti-disturbance ability of the system, and further improve the convergence speed of the system through the linear terms in the integral fast non-singular sliding surface.

2 Related works

(1) Parallel robot

Because of its compact structure, the working space of parallel robot is relatively small, which also makes it more difficult to study than series robot in the early stage.

Reference [4] has done a lot of research on the Delta parallel mechanism, and wants to simplify the mechanism. Finally, the mechanism is simplified by replacing the ball hinge with Hooke hinge, and the stability of the mechanism is improved. Reference [5] put forward the concept of Hexa high-speed manipulator, and its principle is to change the Delta parallel mechanism into a six-branch chain to improve its maneuverability. Reference [6] used intelligent industrial robots to sort on multiple production lines, replacing the original manual operation and improving the sustainability of production line production.

With the large number of practical applications of image processing in industry, the development of machine vision technology sometimes can't meet some specific sorting, detection and recognition needs, and there is another bottleneck in realizing intelligent sorting. As research deepened, researchers began to focus on the field of artificial intelligence and expanded the use of machine learning in industrial production [7]. Machine learning is a science of artificial intelligence. The object of research imitation is the related performance of people in learning, which is converted into computer language to improve the performance of specific algorithms. Its three major elements are data, algorithms and models. There are many branches of machine learning, among which deep learning is the latest research direction and the closest to the initial research goal of machine learning. The goal is to realize that machines have the ability to analyze and solve problems like humans [8]. In addition, deep learning realizes autonomous learning in a data-driven way, and its ability to generalize essential features is higher than that of specific image processing. It performs well in tasks such as search technology, target detection, recognition and classification, data mining, and image segmentation. Sorting robots integrate deep learning technology, which performs well in practical applications, improves sorting efficiency and provides a new way for factories to develop intelligence. Moreover, it has better replaceability for target diversity in sorting, and the cost of factory development and production line is also reduced [9]

(2) Research on trajectory planning and control strategy of parallel robot

The motion performance of the robot is usually closely related to the motion of the end effector, and the motion of the end is transmitted by each branch chain or joint in turn to drive the end to move in the workspace. When the terminal performs the specified task, it moves purposefully. It is necessary to determine the path of the robot according to the task execution, and move along the planned path. In order to improve the motion performance of the mechanism, it is necessary to determine the speed, acceleration and motion law in the motion process. This process is trajectory planning [10]. According to different end execution tasks and whether it is necessary to specify specific paths, it can be divided into point-to-point trajectory planning and continuous path planning. According to different planning coordinate spaces, it can be divided into Cartesian coordinate space planning and joint space planning. The two kinds of spatial planning have certain connection. Nowadays, the application scenarios of parallel robots tend to be diversified and complex. In addition to meeting the constraints of the mechanism itself, according to the trajectory planning optimization indicators, such as execution time, impact on the mechanism, vibration, etc., trajectory planning is mainly divided into: time optimal planning, minimum energy consumption planning and vibration impact optimization. The purpose is to improve the overall performance of the mechanism or reduce the difficulty of

control by improving or combining the motion trajectory [11]. In practical applications, Delta parallel robot is mainly used for quick grasping, sorting or packaging of targets on conveyor belts. In reference [12], while ensuring continuous acceleration and speed and reducing mechanism vibration, the trajectory planning in the workspace was carried out with the shortest working cycle of Delta parallel robot as the goal, and it was concluded that the modified trapezoidal motion law has a short period. Reference [13] proposed a hyperelliptic curve trajectory planning method for the turning point of gate trajectory, which uses high-order polynomial for smoothing. Reference [14] used Lame curve to smooth the gate trajectory, and optimized the trajectory parameters through the change of load energy. Reference [15] used the method of dynamic trajectory programming based on Bézier curve, and used polynomial of degree 3-4-5 to plan the dynamic trajectory. The results show that the residual vibration can be effectively reduced. In reference [16], the arc transition was used at the right angle of the gate trajectory, and the modified trapezoid was used to plan the task trajectory, which reduces the impact of the transition section on the system. In reference [17], the gate trajectory was processed by segments, and the height and length of the trajectory were controlled by polynomial interpolation method for segments, and the optimal period of the trajectory was obtained by improving particle swarm algorithm. Aiming at the problem of unsmooth motion of Delta robot in the process of grasping and placing, reference [18] proposed arc planning to achieve the trajectory in space by using polynomial to plan the obtained angle, so as to obtain the parameters of the end trajectory. Through experiments, the peak value of the end acceleration decreases and the motion tends to be smooth.

In the process of considering the optimal time and energy consumption, the focus of trajectory planning is still on the smoothness and stability of motion. The performance and energy consumption of the currently used motors have been guaranteed, so when the speed is sufficient, trajectory planning is more inclined to smooth the motion curve, stabilize the end and reduce the impact. The core of the stable and accurate operation of Delta parallel robot and the accurate execution of complex tasks lies in the control of the robot, so it is necessary to design an intelligent control strategy with strong robustness and adaptive adjustment. Delta parallel robot has the problems of joint coupling and nonlinear control object, and its control has always been a difficult and hot spot in research [19]. Parallel robots are mainly divided into two types of control, kinematics control and dynamics control. Kinematic control mainly establishes a dynamic connection between the motion relationship between the robot's execution end and the drive end and the drive the drive device, SO as to control device (electromechanical, electro-hydraulic, electromagnetic, etc.) according to the end motion. The dynamic control is controlled by the dynamic model and the end force. Commonly used control strategies include PID control, synovial membrane control, calculated torque control and strategies combined with corresponding control intelligent algorithms [20].

The summary of existing research is shown in Table 1.

Table 1: Summary of existing researches

Research field	Core methods/technologies	Industrial sorting performance indicators	Insufficient
Mechanism optimization	Tiger joint replaces ball joint	Enhance structural stability	The workspace may be limited and there may be insufficient optimization of dynamic performance
optimization	Hexa six branched structure	Enhance maneuverability	The complexity of the structure increases, making it more difficult to control
Machine vision integration	Deep learning object detection	Sorting efficiency ↑, production line cost ↓, adaptability to target diversity ↑	Real time performance is limited by model complexity and relies on a large amount of annotated data
	Correct the law of trapezoidal motion	Shorten the homework cycle	Sudden acceleration change leads to impact vibration
	Super elliptic curve (high-order polynomial smoothing)	Improve the smoothness of turning points	Complex calculation and poor real-time performance
	Lame curve+energy optimization	Reduce load energy fluctuations	Parameter optimization depends on specific scenarios and has weak generalization
Trajectory planning\	B é zier curve+polynomial interpolation	Significantly reduce residual vibration	Insufficient adaptability to dynamic trajectories
	Arc transition+corrected trapezoid	Reduce system impact	Trajectory length increases, sacrificing time efficiency
	Segmented polynomial+improved particle swarm optimization	Optimize cycle	Algorithm convergence is slow, and real-time control is difficult to guarantee
	Arc planning+angle polynomial	Peak acceleration ↓, smoothness of motion ↑	Unresolved robustness issue under external interference
	PID+intelligent algorithm	Accuracy ↑, adaptability ↑	Most of the experiments are in the experimental stage, and the robustness of practical applications is insufficient
Control strategy	SMC (Sliding Mode Control)	Strong anti-interference ability	Severe high-frequency oscillation requires precise modeling
	ESO+SMC combination	Enhanced disturbance estimation capability	ESO is sensitive to noise, and fixed parameters lead to rigid dynamic response

There are three shortcomings in the existing research on sorting control of Delta parallel robots. Firstly, traditional trajectory planning methods rely on preset parameters and are difficult to dynamically adapt to changes in working conditions such as conveyor belt speed fluctuations. Secondly, mainstream control strategies require precise modeling and have limited anti-interference capabilities, resulting in tracking errors (>0.5 mm) or chattering phenomena during high-speed sorting. Thirdly, intelligent algorithms are computationally complex and difficult to meet millisecond level real-time response requirements. The system combining Extended State Observer (ESO) and adaptive control demonstrates significant superiority: ESO can estimate and compensate for unmodeled disturbances in real time, and the adaptive mechanism can dynamically adjust control parameters, achieving a 40% reduction in tracking error and a 60% reduction in vibration amplitude at a sorting frequency of 200 times/minute, while maintaining robustness to $\pm 30\%$ load changes, providing a lightweight solution for high-speed and high-precision sorting.

3 Adaptive control model

A. Overall Design of Improved ST-ESO Controller

The converter is shown in Figure 1. Among them, v_{in} is the input voltage, Q1 and Q2 are the branch power switch tube, L1 and L2 are the branch inductance, and M is the mutual inductance; i_{La} for the inductor current of branch A, i_{Lb} for the inductor current of branch B; D_1 and D_2 are the freewheeling diode, R_a and R_b are the load resistance of the output branch, C_a and C_b are the output capacitor of the converter, d_a and d_b are the duty cycles of the switching tubes Q1 and Q2, respectively.

The overall control design block diagram of the CI-SIDO Buck converter with improved super-twisting ESO is shown in Figure 2.

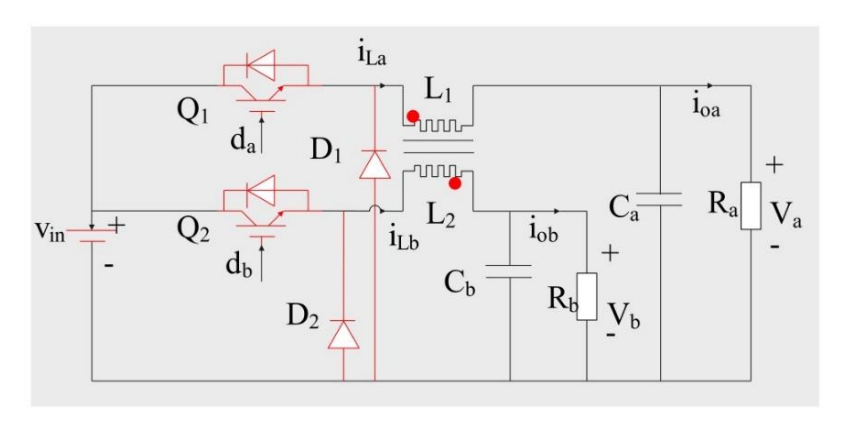


Figure 1: CI-SIDO buck converter circuit topology

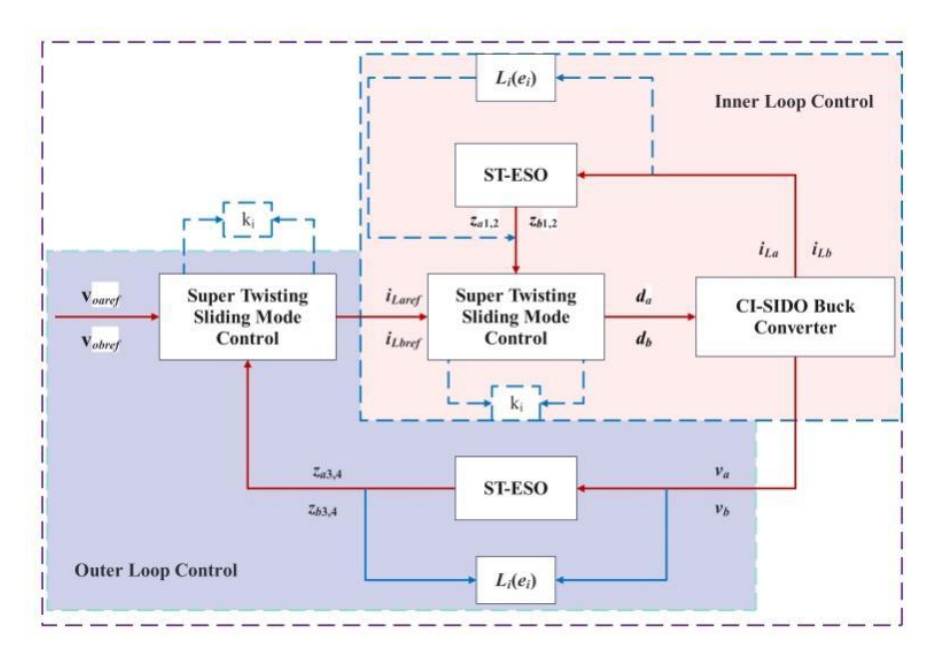


Figure 2: Improved control block diagram of CI-SIDO Buck converter

To further improve the ability of super-twisting sliding mode expanded state observer to observe the total disturbance in the inner and outer loops of CI-SIDO Buck converter and the ability of controller to compensate the total disturbance, an adaptive sliding mode control strategy based on Variable Gain Super-Twisting Expanded State Observer (VGST-ESO) is proposed. Firstly, a hyperbolic function is used to replace the sign function in the super-twisting sliding mode expanded state observer to reduce system chattering, and a variable gain function that can change in real time with the observation error is designed to replace the linear gain of the ST-ESO, so as to improve the observation ability of disturbances. For the super-twisting sliding mode controller, a generalized super-twisting sliding mode algorithm with linear terms is introduced as the reaching law of the system to smooth the system control law, and an adaptive law is designed to weaken the dependence of the generalized super-twisting sliding mode algorithm on the disturbance boundary.

The block diagram of adaptive sliding mode decoupling control based on variable gain super-twisting sliding mode observe is shown in Figure 3. This model can further improve the observation ability of the super-twisting sliding mode observe extended state observer for the total disturbance of the inner and outer loops of CI-SIDO buck converter and the compensation ability of the controller for the total disturbance Firstly, the hyperbolic function is used to replace the sign function in the super-twisting sliding mode observer extended state observer to reduce the chattering of the system. A variable gain function that can change in real time with the observation error is designed to replace the linear gain of ST-ESO, so as to improve the observation ability of disturbance. For the super-twisting sliding mode observer, the generalized super-twisting sliding mode algorithm with linear term is introduced as the reaching law of the system to smooth the system control law, and an adaptive law is designed to weaken the dependence of the generalized super-twisting sliding mode algorithm on the disturbance boundary and improve the anti-disturbance ability of the system. In order to further improve the robustness of the system; In order to further improve the robustness of the system, an integral fast nonsingular sliding surface is designed. The linear term in the integral fast nonsingular sliding surface is used to further improve the convergence speed of the system, improve the overall performance of the system, and ensure the stability and anti-interference performance of the control.

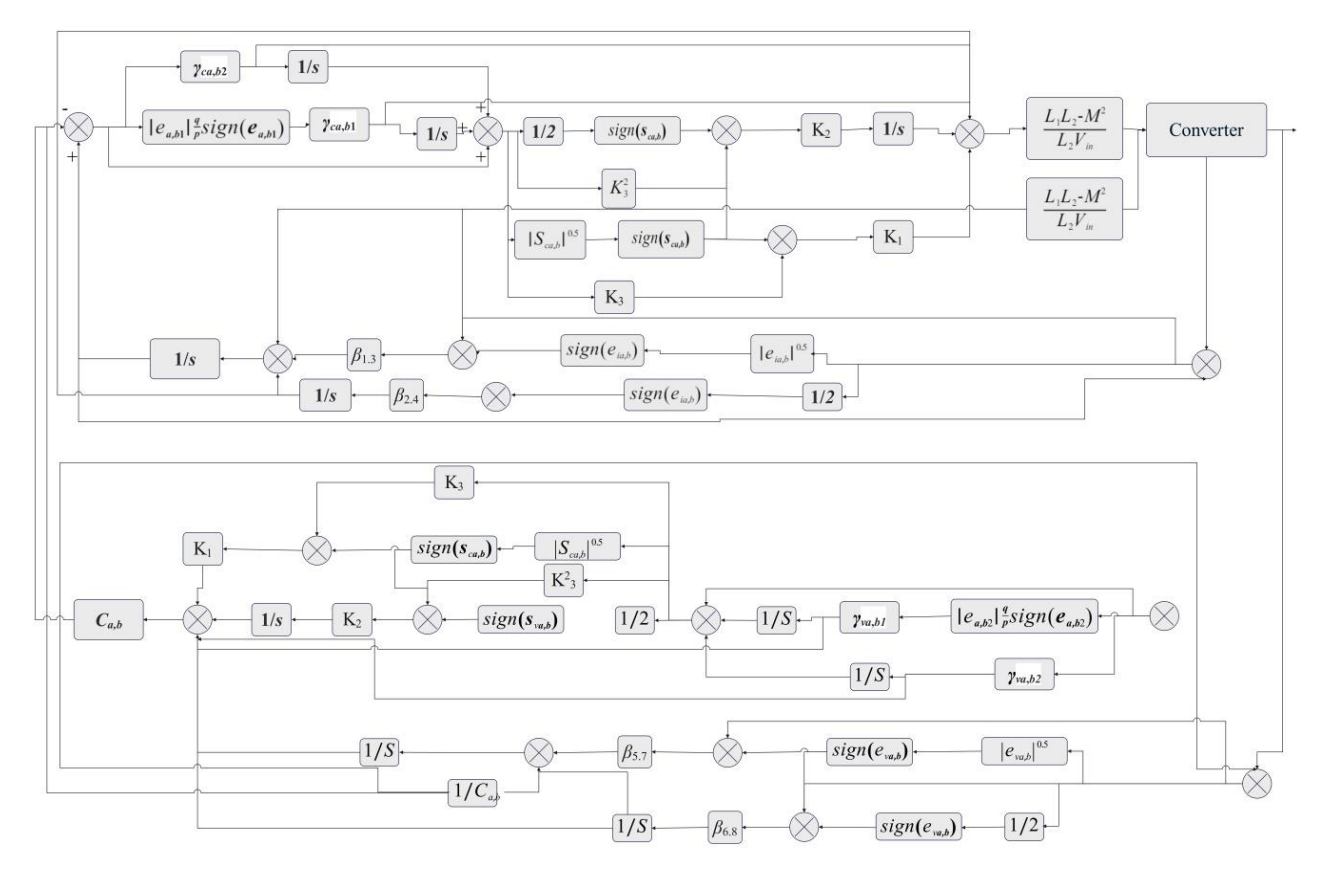


Figure 3: Improved adaptive control block diagram

By normalizing the inductance current, output voltage and other state variables according to the nominal value (such as dividing by the rated current or voltage), the numerical difference of different physical dimensions is eliminated, and the numerical instability caused by too large or too small variable magnitude of the controller gain is avoided. By normalizing, the total disturbances such as inner and outer loop coupling terms and unmodeled dynamics are limited to the effective estimation range of the observer (such as ST-ESO), which ensures that the hyper spiral sliding mode controller can accurately compensate the disturbance and avoid observer saturation or divergence In the normalized model, the ESO gain matrix and the coefficients of the sliding mode control law can be dynamically adjusted based on the normalized state variables, such as dynamically updating the sliding mode surface parameters according to the load changes, so as to enhance the robustness of the system to extreme conditions.

The normalized state variable can avoid the overflow risk of fixed-point operation, and reduce the influence of quantization error on sliding mode chattering, so as to realize the anti overflow processing of discrete algorithm By normalizing the upper and lower limits of the sliding mode control output (e.g., the duty cycle is limited between 0-1), the controller output is prevented from exceeding the physically realizable range under extreme parameters, so as to realize the control of output limiting.

B. Design of Variable Gain Super-Twisting Sliding Mode ESO

The system convergence verification scheme of this article is as follows: the control scheme of the model is selected as the neural approximator enhanced SMC implementation scheme, which adopts RBF neural network dynamic compensation system nonlinearity: taking the inductance current error, capacitance voltage error and their derivatives of Buck converter as network inputs (3 input nodes), the hidden layer is configured with 15 Gaussian radial basis function nodes, and the output layer generates the equivalent control quantity compensation term of sliding mode control; Design an online weight update law using Lyapunov function (learning rate η =0.01) to ensure network convergence and closed-loop stability.

By comparison with super-twisting sliding mode extended state observer (ST-ESO) and linear extended state observer (ESO), it can be seen that ST-ESO has higher observation accuracy and better robustness, but the error term of ST-ESO adopts the switching function integral fast non-singular adaptive super-twisting sliding mode decoupling control number sign, which makes the system have some chattering problems. In order to systematically reduce the chattering problem, a smooth hyperbolic function is used instead of the discontinuous switching function sign.

The switch function sign expression is [21]:

$$sign = \begin{cases} 1, s > 0 \\ 0, s = 0 \\ -1, s < 0 \end{cases}$$
 (1)

It can be seen from Formula (1) that the sign switching function is a discontinuous function. When the switching function sign is used as the sign function of the super-twisting sliding mode expanded state observer, the discontinuous switching control characteristics will be generated with the observation error, resulting in chattering problem and affecting the observation accuracy of the system. Therefore, the smooth hyperbolic function F(e) is used as the switching function. The hyperbolic function F(e) is expressed as [22]:

$$F(e) = \frac{e^{me} - e^{-me}}{e^{me} + e^{-me}}$$
 (2)

The trend of hyperbolic function F(e) is shown in Figure 4.

It can be seen from Formula (2) and Figure 5 that the switching function F(e) is a continuous and smooth function. Different from the symbolic function sign, there are no discontinuities, which can theoretically weaken the buffeting problem and improve the observation ability of generalized supercoil ESO to disturbance.

The super-twisting expanded state observer uses linear gain as the observer gain, and the observation ability of the observer will not change with the observation error in real time, and the system will only converge along a fixed convergence speed. A variable gain function that can change with the observation accuracy in real time is designed to replace the fixed gain of ST-ESO.

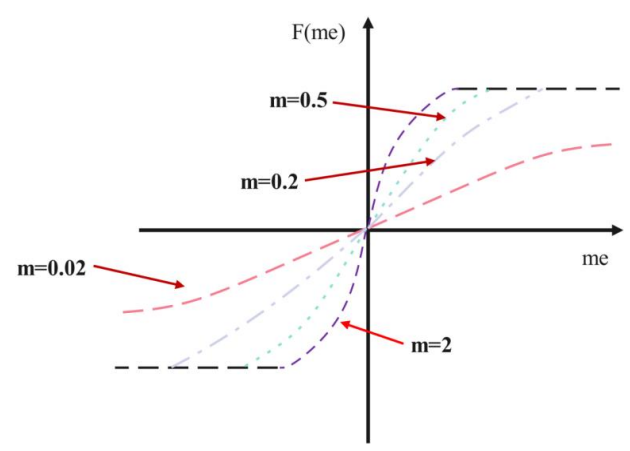


Figure 4: Trajectory plot of hyperbolic function F(e)

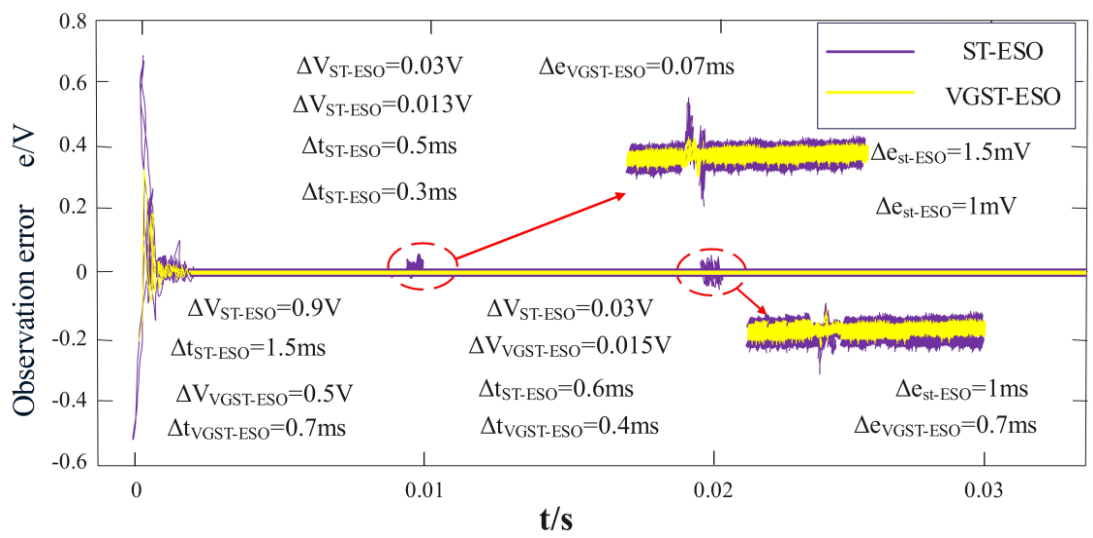


Figure 5: Observation error curve

The improved super-twisting ESO expression is:

$$\begin{cases} e = \theta - y \\ \dot{\theta}_{1} = b_{0}u + \theta_{2} - \beta_{1} \left(\left| e \right|^{\frac{1}{2}} F\left(e \right) + e \right) \\ \dot{\theta}_{2} = -\beta_{2} \left(\frac{1}{2} F\left(e \right) + \frac{3}{2} \left| e \right|^{\frac{1}{2}} F\left(e \right) + e \right) \end{cases}$$
(3)

In the formula, β_1 and β_2 are variable gain functions,

e is the observer error, θ_I is the observed value of Y, and θ_2 is the observed value of the total disturbance.

Nonlinear functions related to error signalsare introduced, combined with disturbance observers to estimate the upper bound of system uncertainty. Finally, the gain variation law is determined through simulation optimization to suppress chattering while ensuring tracking accuracy.

The specific calculation formula obtained is:

$$\begin{cases} \beta_{I} = \sqrt{L(t)} \\ \beta_{2} = \frac{L(t)}{4} \end{cases} \tag{4}$$

The expression of variable gain L(t) is:

$$\dot{L}(t) = \begin{cases} \omega e, e \le \varsigma \\ 0, e > \varsigma \end{cases}$$
 (5)

In the formula, ω and ς are both greater than 0 and are adjustable positive numbers. ς determines the observation accuracy of the improved super-twisting ESO.

The variable gain ST-ESO of the inner loop of the converter current is established as follow [23, 24]:

$$\begin{cases} e_{eI} = \theta_{aI} - x_{cI} \\ \dot{\theta}_{aI} = \frac{L_2 v_{in} d_a}{L_I L_2 - M^2} + \theta_{a2} - \beta_I \left(\left| e_{eI} \right|^{\frac{1}{2}} F\left(e_I \right) + e_{eI} \right) \\ \dot{\theta}_{a2} = -\beta_2 \left(\frac{1}{2} F\left(e_{eI} \right) + \frac{3}{2} \left| e_{eI} \right|^{\frac{1}{2}} F\left(e_{eI} \right) + e_{eI} \right) \\ e_{e2} = \theta_{bI} - x_{c2} \\ \dot{\theta}_{bI} = \frac{L_I v_{in} d_b}{L_I L_2 - M^2} + \theta_{b2} - \beta_3 \left(\left| e_{c2} \right|^{\frac{1}{2}} F\left(e_{c2} \right) + e_{c2} \right) \\ \dot{\theta}_{b2} = -\beta_4 \left(\frac{1}{2} F\left(e_{c2} \right) + \frac{3}{2} \left| e_{c2} \right|^{\frac{1}{2}} F\left(e_{c2} \right) + e_{c2} \right) \end{cases}$$

In the formula, The inner loop observation errors of the a and b branches of the hyper spiral expansion state observer are e_1 and e_2 , respectively, e_{c1} and e_{c2} are the errors between the observed values and the actual values of the inner loop observer of branch a and branch b, respectively. x_{c1} and x_{c2} are the actual values of branch a and branch b of the CI-SIDO Buck converter, β_1 and β_2 are the variable gain functions of the observer of branch a, and β_3 and β_4 are the variable gain functions of the observer of branch b.

The variable gain ST-ESO of the converter voltage outer loop is established as follow [25]:

$$\begin{cases} e_{vI} = \theta_{a3} - x_{vI} \\ \dot{\theta}_{a3} = \frac{1}{C_a} + \theta_{a4} - \beta_5 \left(\left| e_{vI} \right|^{\frac{1}{2}} F(e_{vI}) + e_{vI} \right) \\ \dot{\theta}_{a4} = -\beta_6 \left(\frac{1}{2} F(e_{vI}) + \frac{3}{2} \left| e_{vI} \right|^{\frac{1}{2}} F(e_{vI}) + e_{vI} \right) \\ e_{v2} = \theta_{b3} - x_{v2} \\ \dot{\theta}_{b3} = \frac{1}{C_b} i_{L2} + \theta_{b4} - \beta_7 \left(\left| e_{v2} \right|^{\frac{1}{2}} F(e_{v2}) + e_{v2} \right) \\ \dot{\theta}_{b4} = -\beta_8 \left(\frac{1}{2} F(e_{v2}) + \frac{3}{2} \left| e_{v2} \right|^{\frac{1}{2}} F(e_{v2}) + e_{v2} \right) \end{cases}$$

$$(7)$$

In the formula, e_{vI} and e_{v2} are the errors between the observed values and the actual values of the voltage outer loop observer of branch a and branch b, respectively, x_{vI}

and x_{v2} are the actual values of branch a and branch b, β_5 and β_6 are the variable gain functions of the observer of branch a, and β_7 and β_8 are the variable gains of the observer of branch b.

By analyzing Formulas (4) and (5), it can be seen that the variable gain function designed in this paper changes in real time according to the observation error. When the observation error is larger, the observer gain coefficient increases, which can speed up the convergence speed of the observer. When the observation error becomes smaller, the observer gain value is correspondingly reduced, thus avoiding the over-estimation of the observer.

For the fairness of the comparison, the controllers are all the proposed super-twisting sliding mode controllers, and a simulation platform based on Matlab/Simulink is built to simulate and compare the performance of the observers.

The observation error comparison between variable gain super-twisting sliding mode ESO and linear super-twisting sliding mode ESO is shown in Figure 5.

In the system startup stage, the convergence overshoot of ST-ESO is 0.9 V, the convergence time is 1.5 ms, and the observation error is 1mV. The convergence overshoot of VGST-ESO is 0.5 V, the convergence time is 0.7 ms, and the observation error is 0.7 mV. At 0.01 s disturbance, the convergence overshoot of ST-ESO is 0.03 V, the convergence time is 0.5 ms, and the observation error is 1.5 mV. The convergence overshoot of VGST-ESO is 0.013 V, the convergence time is 0.3 ms, and the observation error is 1mV. When the system is disturbed at 0.02 s, the convergence overshoot of ST-ESO is 0.03 V, the convergence time is 0.6 ms, and the observation error is 1mV. The convergence overshoot of VGST-ESO is 0.015 V, the convergence time is 0.4 ms, and the observation error is 0.7 mV.

By comparing the convergence overshoot, convergence speed and observation error in the start-up stage and when the system is disturbed, it can be seen that the overall performance of VGST-ESO is superior to that of ST-ESO. The improved variable gain super-twisting sliding mode expanded state observer designed can adaptively adjust the observer gain according to the observation error.

The observation errors \dot{e}_1 and \dot{e}_2 of the super-twisting expanded state observer are respectively:

$$\begin{cases} \dot{e}_{1} = e_{2} - l_{1}\phi_{1}\left(e_{1}\right) \\ \dot{e}_{2} = -l_{2}\phi_{2}\left(e_{1}\right) - f \end{cases}$$
(8)

In the formula, $\phi_{I}(e_{I}) = |e_{cI}|^{\frac{1}{2}} sign(e_{I}) + e_{cI}$ and $\phi_{2}(e_{I}) = \frac{1}{2} sign(e_{cI}) + \frac{3}{2} |e_{cI}|^{\frac{1}{2}} sign(e_{cI}) + e_{cI}$.

The Lyapunov function is defined as:

$$V_{3} = \frac{I}{L(t)^{2}} \tau^{T} G(t) \tau \tag{9}$$

In the formula,

$$\tau^{T} = \left(\phi_{I}\left(e_{cI}\right), e_{c2}\right), G\left(t\right) = \frac{1}{2} \begin{bmatrix} 4\beta_{2}\left(t\right) + \beta_{I}^{2}\left(t\right) & -\beta_{I}\left(t\right) \\ -\beta_{I}\left(t\right) & 2 \end{bmatrix}.$$

By taking the derivative of Formula (9), it can be obtained:

$$\dot{V}_{3} = \frac{d}{dt} \frac{1}{L(t)^{2}} \tau^{T} G(t) \zeta \tag{10}$$

By expanding Formula (10), it can be obtained:

$$\dot{V}_{3} = \tau^{T} \frac{d}{dt} \left(\frac{1}{L(t)^{2}} G(t) \tau \right) + \frac{1}{L(t)^{2}} \left(\dot{\tau}^{T} G(t) \tau + \tau^{T} G(t) \dot{\tau} \right)$$
(11)

To prove that \dot{V}_3 is convergent, it is only necessary to

prove that both
$$au^T \frac{d}{dt} \left(\frac{1}{L(t)^2} G(t) \tau \right)$$
 and

$$\frac{1}{L(t)^2} (\dot{\tau}^T G(t) \tau + \tau^T G(t) \dot{\tau})$$
 are negative constants to

prove that the validation system is convergent. Here, $\dot{V}_{\scriptscriptstyle 3a}$ is represented as two parts, to be verified separately,

Decompose the total Lyapunov function V_3 into two components V_{3a} and V_{3b} , corresponding to the stability of the controller and observer, respectively Provide intermediate process steps for global stability through component stability.

$$\dot{V}_{3a} = \tau^{T} \frac{d}{dt} \left(\frac{1}{L(t)^{2}} G(t) \tau \right), \dot{V}_{3b} = \frac{1}{L(t)^{2}} \left(\dot{\tau}^{T} G(t) \tau + \tau^{T} G(t) \dot{\tau} \right) \text{ obtained } |e_{cl}|^{\frac{1}{2}} \leq ||\tau||_{2}. \text{ Then, it can be obtained:}$$

, then Formula (11) is re-expressed as:

$$\dot{V}_{3} = \dot{V}_{3a} + \dot{V}_{3b} \tag{12}$$

By substituting Formula (4) and
$$G(t) = \frac{1}{2} \begin{bmatrix} 4\beta_2(t) + \beta_1^2(t) & -\beta_1(t) \\ -\beta_1(t) & 2 \end{bmatrix}$$
 into Formula (12),

 \dot{V}_{3a} in the Formula (12) can be expressed as:

$$\dot{V}_{3a} = \frac{1}{2} \tau^{T} \frac{d}{dt} \begin{bmatrix} 2L(t)^{-1} & -L^{\frac{-5}{2}}(t) \\ -L(t)^{\frac{-5}{2}} & 2L^{-2} \end{bmatrix} \tau$$
 (13)

From Formula (13), it can be obtained:

$$\dot{V}_{3a} = \frac{1}{2} \tau^{T} \frac{d}{dt} \begin{bmatrix} -2L(t)^{-2} & \frac{5}{2}L^{\frac{-7}{2}}(t) \\ \frac{5}{2}L(t)^{\frac{-7}{2}} & -4L^{-3} \end{bmatrix} \dot{L}\tau$$
 (14)

L is the actual inductance, and \dot{L}_{τ} is the nominal value of the inductance used for decoupling controller design.

It is a known design parameter in the controller formula, aimed at offsetting the inductance dynamics of the actual system in the control law.

When
$$\dot{L} > 0$$
 and $L(0) > \frac{5\sqrt{2}}{8}$ are satisfied, $\dot{V}_{3a} < 0$,

and \dot{V}_{3a} is negative definite at this time. The negative definiteness of \dot{V}_{3a} is proved as follows:

According to Formula (11), τ can be expressed as:

$$\dot{\tau} = \frac{1}{|e_{cI}|^{\frac{1}{2}}} A \tau + B^T \tag{15}$$

In the formula,
$$A = \begin{bmatrix} -\beta_1 & I \\ 2 & 2 \\ -\beta_2 & 0 \end{bmatrix}, B = \begin{bmatrix} 0 & f \end{bmatrix}.$$

Substituting Formula (15) into Formula (12), it can be obtained V_{3h} as:

$$\dot{V}_{3b} = \frac{1}{L(t)^2} \left(-|e_{cI}|^{\frac{-1}{2}} \tau^T Q \varsigma + 2\tau^T G B^T \right)$$
 (16)

is

$$Q = \frac{\sqrt{L(t)}}{2} \begin{bmatrix} \frac{3}{2}L(t) & -\sqrt{L(t)} \\ -\sqrt{L(t)} & 1 \end{bmatrix}.$$

From Formula (16), it can be obtained:

$$\dot{V}_{3b} = \frac{1}{L(t)^2} \frac{1}{|e_{cI}|^{\frac{1}{2}}} \left(-\tau^T Q \tau + 2 |e_{cI}|^{\frac{1}{2}} \tau^T G B^T \right)$$
(17)

From the Euclidean norm $\|\tau\|_{2}^{2} = |e_{cl}| + e_{e2}^{2}$, it can be

$$\dot{V}_{3b} \le -\frac{1}{L(t)^2} \frac{\|\tau\|_2^2}{|e_{-t}|_2^{\frac{1}{2}}} (\lambda_{min}(Q) - 2\delta_I \lambda_{max}(P(t)))$$
(18)

When L(t) satisfies the following inequality:

$$\lambda_{\min}(Q) - 2f\lambda_{\max}(G(t)) > 0 \tag{19}$$

It can be obtained:

$$\dot{V}_{3b} \le -v V_3^{\frac{1}{2}} \tag{20}$$

In the formula,
$$v = -\frac{\lambda_{min}(Q) - 2\delta_I \lambda_{max}(G(t))}{L(t)^2 \lambda_{max}^{1/2}(G(t))}$$
.

From Formula (14) and Formula (20), we can see that the designed $V_{\scriptscriptstyle 3a}$ and $V_{\scriptscriptstyle 3b}$ are negative definite and the system is convergent.

In the above algorithm steps, a Lyapunov function containing the dynamic equation of observation error is constructed. By taking the derivative and substituting it into the control law of the hyper spiral algorithm, the finite time stability condition is satisfied to ensure that the observation error converges to the zero neighborhood within a finite time. This process combines the linear error dynamic analysis of traditional ESO with the nonlinear robustness of the hyper spiral algorithm, ultimately achieving accurate tracking of composite disturbances by the observer by adjusting the gain parameter.

The application of the improved super-twisting sliding mode observer (ST-ESO) in the field of power electronics parallel robot control essentially interdisciplinary method transfer by establishing dynamic equivalent models of two types of systems. Specifically, at the variable mapping level, the inductance current of the Buck converter needs to be mapped to the output torque of the robot joint motor, and the steady-state characteristics of the output voltage correspond to the spatial pose accuracy of the end effector; In terms of disturbance handling, sudden load changes in the power system are redefined as external load disturbances and joint nonlinear friction during robot operation. The 8 adaptive gain parameters of the original controller need to be reconstructed into the inertia matrix adjustment coefficient and Coriolis force compensation coefficient in the robot dynamics model, while retaining the finite time convergence characteristics of the hyper helix algorithm. When implementing hardware, a three-level collaborative architecture of "power conversion servo drive mechanical execution" needs to be constructed. The clock synchronization between the power observer (100 µs cycle) and the motion controller is achieved through FPGA. The core innovation lies in the parameterized coupling of power electronic control theory and robot motion control through isomorphism analysis of dynamic equations.

4 Test study

C. Test methods

The experimental platform of Delta robot dynamic sorting and related hardware selection are explained, and the flow of dynamic sorting system and the data communication format between visual inspection system and robot sorting system are designed. The experimental platform of Delta robot dynamic sorting includes visual

inspection system, robot sorting system and conveying system. The end effector and its supporting equipment are shown in Figure 6. The vacuum suction cup needs the cooperative work of air compressor, vacuum generator and solenoid valve to realize the function of absorbing workpieces, in which the air compressor and vacuum generator generate suction, and the solenoid valve controls the opening and closing of airflow.

The suction cup actuator is PU series pneumatic finger produced by SMC in Japan, the solenoid valve is 5 W direction control solenoid valve produced by AIRTAC in Taiwan, the vacuum generator is CGO vacuum generator produced by CKD in Japan, and the air compressor is GSR silent air compressor produced by gree in China.

The industrial camera is installed above the conveyor belt through a camera bracket. It ensures that the workpiece passes through the camera field of view before reaching the robot grabbing area during the movement of the conveyor belt. In addition, the installation height of the camera is adjusted according to the size of the conveyor belt to ensure that the width of the conveyor belt is within the camera field of view to prevent the workpiece from exceeding the camera field of view. The position of the camera is kept at a certain distance from the robot to avoid interference with the robot's movements. The light source is installed under the camera and equipped with a controller that can adjust the brightness of the light source to adjust the appropriate brightness according to the experimental object and experimental environment. The industrial camera and light source are fixed on the conveyor belt by a suitable bracket. The hardware composition of the machine vision inspection system is shown in Figure 7.

The model of the computer is Dell precision, the industrial camera is basiler ace, the light source is Hamamatsu 119050, and the bracket is thorlabs k100, Cable matters USB3.0 A-B cable is selected for USB3.0 cable.

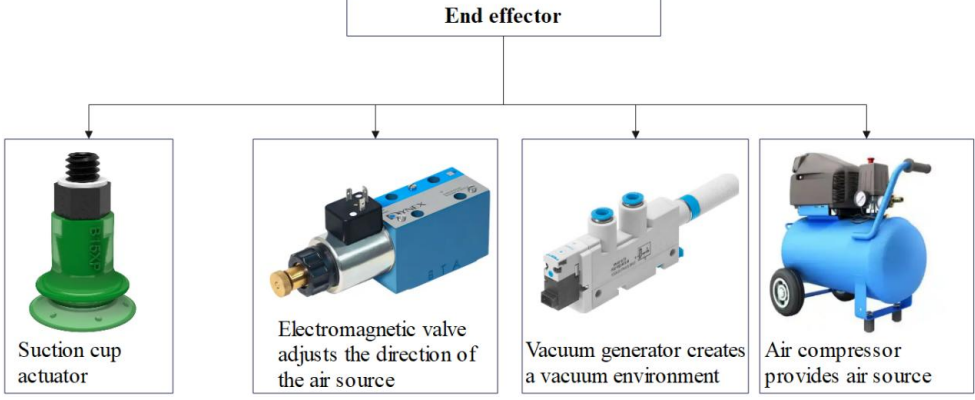


Figure 6: Hardware composition of terminal actuator

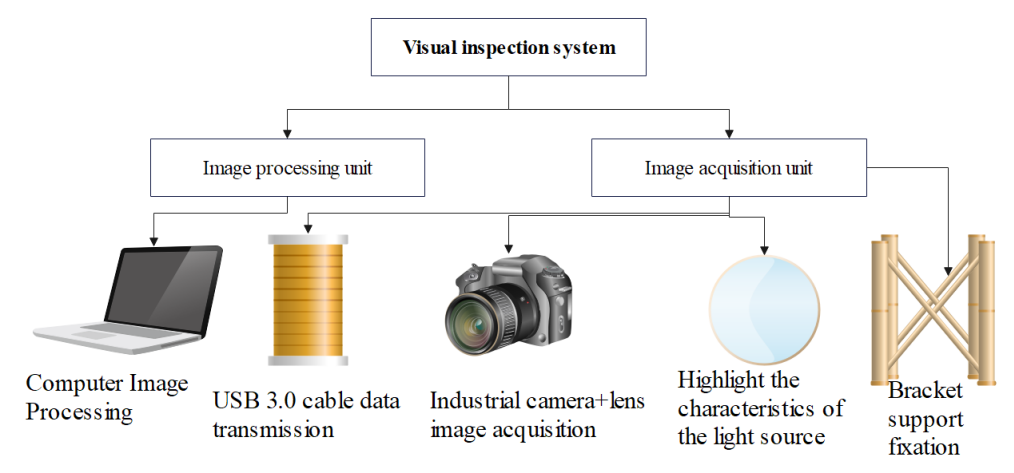


Figure 7: Hardware composition of visual inspection system

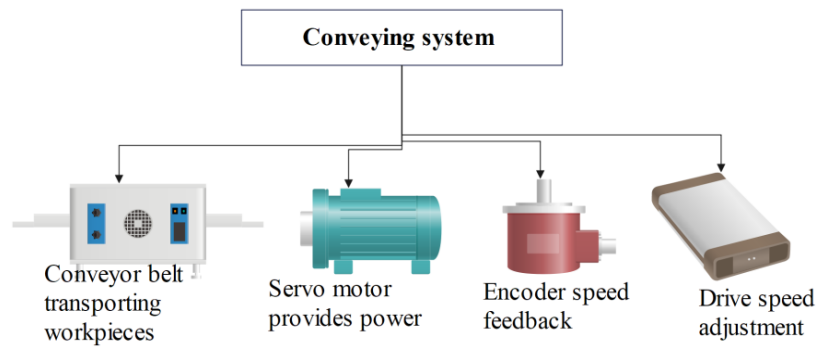


Figure 8: Composition of conveying system

The composition of the conveying system is shown in Figure 8. The installation position of the conveyor belt is located in the grasping area of the Delta robot, and it avoids being close to the edge of the working range of the Delta robot to prevent the Delta robot from exceeding its working range during the grasping of the workpiece. The servo motor is installed on one side of the driving drum of the conveyor belt. The encoder is installed on the opposite side of the driving drum through a coupling to ensure synchronization with the rotation of the conveyor belt drum and realize real-time monitoring.

The motor is Panasonic A4 servo motor, the encoder is Omron e6b2 incremental encoder, the driver is Yaskawa sigma-7 servo driver, and the conveyor belt is fujilay f conveyor belt.

The dynamic sorting experimental platform includes visual inspection system, robot sorting system and conveying system. Each system cooperates with each other to realize the identification, positioning, grasping and placement of the target workpiece on the conveyor belt. The image processing unit identifies and locates the workpiece image acquired by the image acquisition unit, identifies the workpiece using the YOLOv5 target detection model. YOLOv5 is chosen as the target detection model for robot sorting experiments mainly due to its comprehensive advantages in speed, accuracy, and industrial adaptability. The lightweight architecture of YOLOv5 can achieve high frame rate detection of 140 FPS, meeting the real-time requirements of dynamic grabbing of conveyor belts. Its Focus structure and PANet feature pyramid can effectively identify small-sized workpieces and enhance robustness to occlusion and lighting changes through Mosaic data augmentation. Compared to other models, YOLOv5 is more convenient to deploy on embedded devices, and transfer learning only requires 300 annotated samples to achieve mAP@0.5 =0.89, significantly reducing engineering costs. And then locates the workpiece according to the workpiece contour using the visual positioning algorithm. Before image processing, the camera parameters need to be calibrated and the workpiece data set needs to be trained to ensure the accuracy of the visual inspection system's detection and recognition and the accuracy of positioning. Moreover, the visual inspection system identifies and positions the workpiece, and sends the category and position information of the workpiece to the robot sorting system through Socket communication, and the robot sorting system stores the workpiece information in the queue to be grasped. When the workpiece enters the robot grasping area, the robot sorting system controls the Delta robot to grasp the workpiece in an appropriate posture according to the workpiece position information sent by the visual inspection system, and places the workpiece in the corresponding position according to the category information of the workpiece. The dynamic sorting process is shown in Figure 9.

The 3 +1 degree of freedom Delta parallel robot developed in the laboratory is shown in Figure 10. The whole robot is installed in an aluminum alloy frame.

Using a fixed frequency of 1 kHz (such as PWM control) and precise timer configuration, the universal timer (TIM2-TIM5) of the STM32 series microcontroller can output 4 PWM channels and achieve duty cycle adjustment through register configuration.

The model of the microcontroller is STM32F103, with an ARM Cortex-M core that supports real-time control and integrates peripherals such as ADC and timer. It is suitable for high-frequency sampling and signal processing.

Select a combination of Siemens V20 frequency converter and PLC (such as CPU ST30), set the frequency and process the start stop logic through RS485 communication A pre-low-pass filter (such as LM324 operational amplifier) is used to suppress high-frequency noise. The MCU adopts sliding average or IIR filtering algorithm, combined with ADC anti aliasing design to reduce the influence of thermal noise and 1/f noise.

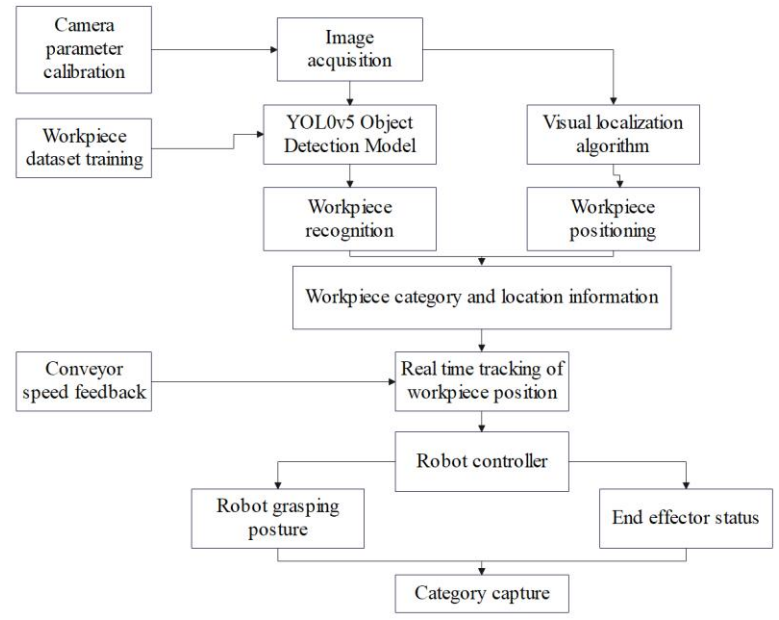


Figure 9: Dynamic sorting process

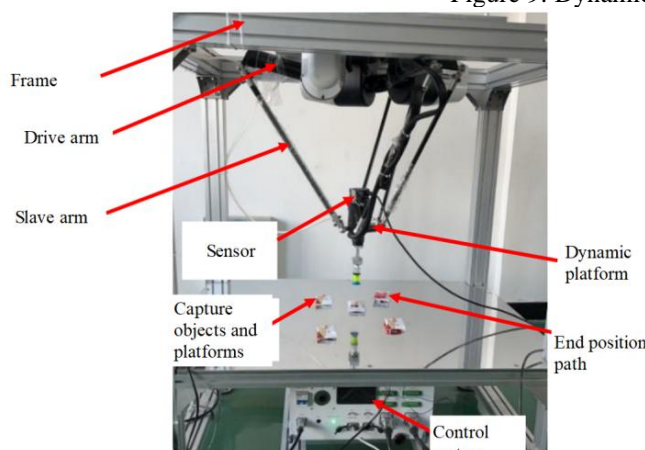


Figure 10: Delta high-speed parallel robot

The control scheme chosen for this model is a neural approximator enhanced SMC implementation scheme, which uses RBF neural network to dynamically compensate for system nonlinearity: taking the inductance current error, capacitance voltage error and their derivatives of Buck converter as network inputs (3 input nodes), configuring 15 Gaussian radial basis function nodes in the hidden layer, and generating equivalent control compensation terms for sliding mode control in the output layer; Design an online weight update law

using Lyapunov function (learning rate η =0.01) to ensure network convergence and closed-loop stability.

The observer bandwidth ω is set to $1/5\sim1/3$ of the system switching frequency, and dynamically adjusted during actual testing. The initial value of the gain slope Zeta is taken as $50\sim100$ rad/V • s.

D. Results

The trajectory diagram of the end effector is shown in Figure 11, and the velocity curve is shown in Figure 12.

End position of The model constructed in this paper is an improved ST-ESO control model, which is named IM-ST-ESO. On the built parallel robot prototype experimental platform for string fruit sorting, the proposed method is compared with the fixed switching gain sliding mode control using online identification of load moment of inertia and the integral adaptive sliding mode control without online identification of load moment of inertia, and objects of different weights are sorted, as shown in Figure 13.

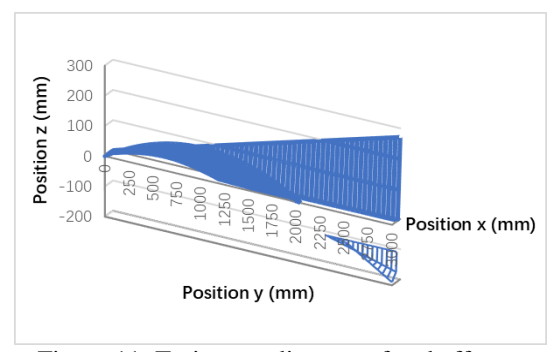


Figure 11: Trajectory diagram of end effector

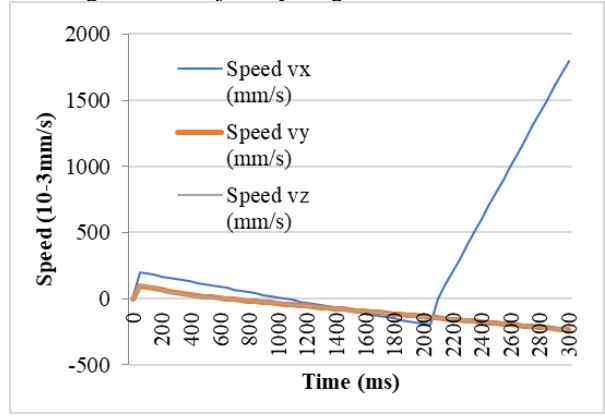
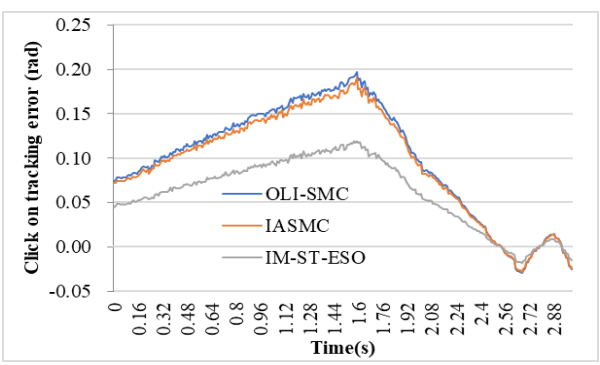
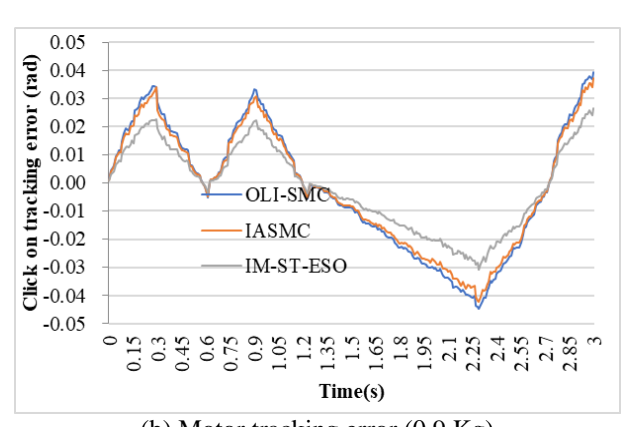
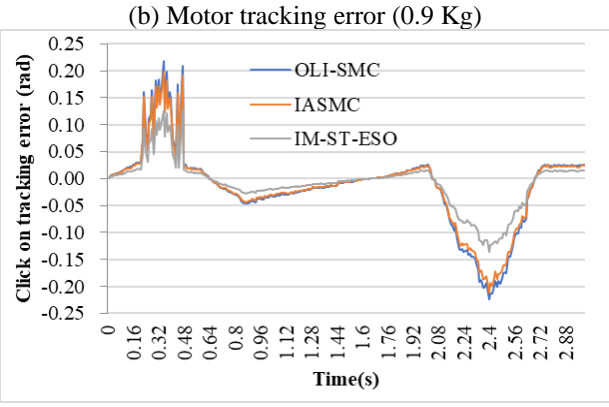


Figure 12: Speed curve



(a) Motor tracking error (0.6 Kg)





(c) Motor Tracking Error (1.5 Kg object winding)

Figure 13: Branch motor tracking error

The root mean square error of the motor and the maximum error when the system is in steady state are shown in Table 2.

Table 2: Root mean square error of motor and maximum error when system is in steady state

	0.6 Kg	0.6 Kg	0.9 Kg	0.9 Kg	1.5 Kg	1.5 Kg
Controller	×10 ⁻³ MSSE/rad	×10 ⁻³ RMSE/rad	×10 ⁻³ MSSE/rad	×10 ⁻³ RMSE/rad	×10 ⁻³ MSSE/rad	×10 ⁻³ RMSE/rad
OLI-SMC	15.05	6.93	22.08	9.80	23.66	10.69
IM-ST-ESO	13.96	4.26	15.74	5.74	19.01	7.52
IASMC	22.08	10.10	29.80	13.86	33.26	14.75

Table 3: Calculation load data of motor

Controller type	Simulation time (seconds)	CPU utilization (%)	Memory consumption (MB)	Iterations (Times)		
OLI-SMC	12.16	68.875	204.25	4560		
IM-ST-ESO	7.79	43.035	152	3040		
IASMC	17.67	85.215	294.5	6175		

Table 4: Performance comparison data of different controllers

Controller type	MSSE	RMSE	CPU usage	Memory usage (MB)	Running time (ms)
IM-ST-ESO	0.0025	0.0498	15%	2.8	2.3
OLI-SMC	0.0032	0.0567	18%	3.2	2.6
IASMC	0.0029	0.0523	16%	3	2.4

Table 5: Results of ablation experiment

Group	Overshoot (%)	Adjustment time (ms)	Steady state error (mV)	Anti disturbance recovery time (ms)
Complete IM-ST-ESO	0.8	1.8	5	2.2
Remove hyperbolic function	2.1	3.5	12	4.7
Fixed gain	1.5	2.9	8	3.8
Remove SMC adaptive rule	3.2	6.4	18	8.1

The calculation burden of the above model is shown in Table 3.

The model constructed in this study is used to sort out defective products from the product. The test object is 750 products, of which 150 defective products are mixed. The experimental scale design for selecting 750 products (including 150 defective products) has clear statistical basis and engineering practicality. The 150 defective products account for 20% of the total sample, which is in line with the typical non-conformance rate range (5%-25%) in industrial scenarios and can effectively simulate the real production line environment. At a 95% confidence level, the confidence interval width of the 20% defective product ratio needs to be controlled within \pm 3%. The sample size of 750 is slightly higher than the calculated value of 683, which can ensure that the statistical error of sorting accuracy is $\leq 3\%$ and meet the engineering accuracy requirements Conduct 2 repeated experiments for each of the 3 transmission speeds, requiring a total of 6 sets of data. Each group is allocated 125 samples, with a constant proportion of defective products, that is, each group contains 25 defective products. Overall, the sample size design of 750 meets the three core requirements of statistical significance, group comparability, and engineering feasibility, providing a scientific basis for sorting performance evaluation.

The performance comparison data of different controllers are shown in Table 4.

Results of ablation experiment is shown in Table 5.

At the beginning of the test, they are placed on the conveyor belt at a uniform speed, and the parallel robot is used for sorting. In addition, the defective products are picked up on another conveyor belt, and two grasping tests are performed for each of the three conveyor speeds

(with a minimum speed limit). There are six groups of tests in total, and the test data are shown in Table 6.

Table 6: Product dynamic recognition and capture results

ruste of 110duct dynamic recognition and capture results						
Number of	Transfer speed	Recognition rate	Grabbing rate			
groups	(mm/s)	(%)	(%)			
1	150	96.53	96.53			
2	130	97.35	96.53			
3	250	96.53	95.70			
4	250	95.70	95.70			
5	350	93.23	91.58			
6	330	94	91.58			

The core idea of combining the improved ST-ESO to optimize the robot's motion trajectory is to estimate and compensate for the total system disturbance in real time through ST-ESO, including model uncertainty, external interference, and unmodeled dynamics. Based on this, a time energy dual objective optimization algorithm is used to generate smooth trajectories, which are dynamically adjusted in conjunction with model predictive control (MPC). In specific implementation, an accurate dynamic inverse model is first constructed using the high-order disturbance observation capability of ST-ESO. Then, trajectory continuity is ensured through fifth order spline interpolation. Finally, the control variables are corrected online according to the disturbance estimation value output by the observer, and the trajectory optimization of the other three methods is achieved through adaptive control.

In the actual operation of Delta robot, the sorting and picking frequency is 120 times/min, and each cycle is 0.50 s. However, considering that the actions of each cycle include picking and placing, the actual time of a single action of picking and placing should be 0.25 s. The optimization results of different methods for the running time of Delta robot are shown in Table 7.

Table 7: Optimization results of delta robot runtime by different methods

Methods	Time before optimization (s)	Time after optimization (s)
Literature [21] (A SVM recognition algorithm based on the fusion of grayscale)	0.25	0.239
Literature [24] (Visual servoing control)	0.25	0.236
Literature [25] (Multi-sensor cyber-physical sorting system)	0.25	0.234
Methods in this paper	0.25	0.231

Table 8: Optimization results of delta robot operation impact by different methods

	1 1	
Method	Average impact before optimization (/(°) · s-3) * 10 ⁶	Average impact after optimization $(/(^{\circ}) \cdot s-3) * 10^{6}$
Literature [21] (A SVM recognition algorithm based on the fusion of grayscale)	2.23	0.481
Literature [24] (Visual servoing control)	2.23	0.466
Literature [25] (multi-sensor cyber-physical sorting system)	2.23	0.463
Methods proposed in this paper	2.23	0.441

The optimization results of different methods on the running impact of Delta robot are shown in Table 8.

The time-domain waveform diagram is shown in Figure 14.

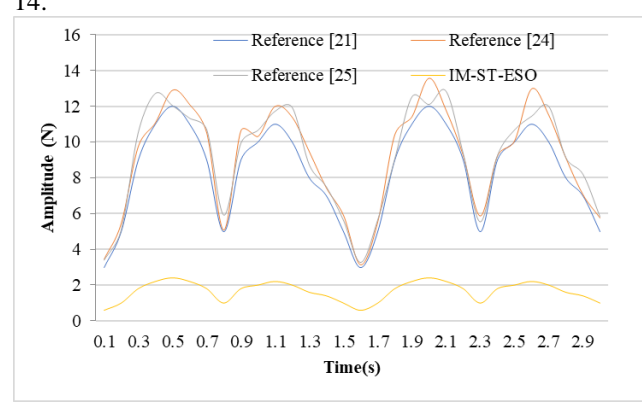


Figure 14: Time domain waveform diagram

In order to compare the average current decoupling control and the sliding mode decoupling control based on ESO in the case of anti load disturbance, the load of branch A and B is mutated respectively. When the output current of one branch of branch A and B changes to 1a \rightarrow >2a \rightarrow >1a, the load of the other branch remains unchanged, and the cross influence between output branches a and B and the dynamic performance of the system under load disturbance are observed through an oscilloscope.

Table 9 shows the experimental results of average current control and sliding mode decoupling control based on ESO against the load disturbance of branch a.

Table 9: Comparison of Different Decoupling Control **Experimental Results**

Control type	Input voltage disturbance (V)	Output branch	Overshoot voltage (V)	Overshoot time (MS)
Avamaga	45→35	A branch	5	18.7
Average current	45→33	B branch	2.5	15.3
control	35→55	A branch	5.5	18.7
[1]		B branch	3	15.3
ESO+sli ding mode	45→35	A branch	3	8.5
		B branch	1.5	6.8
	35→55	A branch	3	6.8
		B branch	2	5.1

The evaluation of the implementation scheme of neural approximator enhanced SMC is shown in Table 10.

Table 10: Evaluation of SMC implementation scheme enhanced by approximator

Experimental condition	Overshoot (V)	Ripple amplitude (relative unit)
Traditional SMC	1.2	1.0 (baseline value)
Neural approximator enhances SMC	0.45	0.6 (reduced by 40%)

To further verify the dynamic control effect of the model in this article, the following is added on top of the calibrated weight (0.6/0.9/1.5 kg):

Instantaneous impact load: +20% sudden weight change (0.48-0.72 kg) of random duration (0.1-0.5 s), continuous fluctuation load: sinusoidal disturbance (amplitude+15%, frequency 0.5-2 Hz). The base speed is set according to the working conditions, superimposed with Gaussian noise (σ=10% calibration value), the trajectory period is randomly shifted by $\pm 5\%$, and a pulse disturbance of 0.5 m/s² is randomly inserted. Random bandwidth vibration of 0-50 Hz is applied through the exciter. The experimental results are shown in Table 11.

Table 11: Random perturbation test results

Testing Team	Load (kg)	Speed disturb ance σ	RMS error (rad)	Steady state maximum error (rad)	Main peak of spectrum (Hz)
Reference group (0.6 kg)	0.60±0 %	0%	0.0021	0.0043	-
Load mutation group	0.54–0 .72	5%	0.0048	0.0097	12.5
Motion disturbanc e group	0.60±2 %	15%	0.0035	0.0062	8.3
Composite disturbanc e group (0.9 kg)	0.81–0 .99	10%	0.0067	0.0124	18.6/35.2

E. Analysis and Discussion

By comparing the root mean square error of the branch motor tracking error and the maximum error when the system is in steady state in Figure 13 and Table 2, it can be seen that when the sorting load of the string fruit sorting parallel robot is unknown and changes dynamically, compared with the integral adaptive sliding mode control method that does not use online identification of the load moment of inertia and the steady-state switching gain sliding mode control method that uses online identification of the load moment of inertia.

In Table 3, IM-ST-ESO has the lowest simulation time and memory consumption, mainly due to its adaptive gain ESO, which can effectively reduce the additional calculation caused by parameter mismatch. In addition, the number of iterations is significantly lower than that of other controllers, indicating that the algorithm has faster convergence speed and is suitable for scenes with high real-time requirements.

The simulation time and CPU utilization of OLI-SMC are at a medium level, indicating that its algorithm complexity is moderate. The higher number of iterations may be related to the chattering suppression mechanism of sliding mode control, which needs to be stabilized by high-frequency switching, resulting in increased computational resource consumption

IASMC has the highest simulation time and memory

consumption, mainly due to its combination of integral operation and adaptive parameter adjustment, resulting in a significant increase in algorithm complexity. The higher number of iterations further verifies that it needs to optimize the parameters many times in the convergence process, and the computational efficiency is low.

From the comparison of Table 4, the ST-ESO controller performs the best in control accuracy (MSSE 0.0025, RMSE 0.0498), computational efficiency (CPU 15%, memory 2.8MB), and real-time performance (running time 2.3 ms), with significantly better overall performance than OLI-SMC and IASMC. Among them, OLI-SMC is the weakest performing solution among the three due to its high resource consumption (CPU 18%, memory 3.2MB) and slow response (2.6 ms), while IASMC is in the middle in various indicators, but its balance may be applicable to some scenarios where performance requirements are not strict. This result indicates that the improved ST-ESO has better stability and engineering applicability in Buck converter control.

In Table 5, the hyperbolic function has a 162% increase in overshoot and a 114% extension in anti-interference recovery time, demonstrating the crucial role of hyperbolic ESQ in suppressing nonlinear disturbances. Fixed gain defect: Steady state error increases by 60%, indicating that adaptive gain can dynamically optimize parameters to cope with load changes. Lack of adaptability in SMS: The adjustment time deteriorates by 255%, highlighting the necessity of adaptive rules for rapid convergence. Overall, the improved ST-ESO modules have significant synergistic effects, with hyperbolic ESO and SMC adaptive rules contributing the most to dynamic performance, while fixed gain mainly affects steady-state accuracy.

In Table 6, when the speed of the conveyor belt is between 150 and 250 mm/s, the identification rate and grasping rate of defective products are above 96%, which is within the allowable error of the project. However, when the speed becomes 350 mm/s, the recognition rate and grasping rate will drop below 95%, which will have a great impact on the quality of sorting. Before entering the sorting process, the movement speed of the products in this project in the previous process is generally between 130-250 mm/s. Therefore, this sorting system fully meets the requirements of the project, can adapt to different production speeds of products, and has certain accuracy and reliability.

In Table 7, the running time performance of optimized Delta robot in reference [3] is poor, and the optimization degree is the lowest. A more effective trajectory cannot be found. The methods in references [8] and [15] have a certain degree of optimization effect and can shorten the exercise time to a certain extent, but the effect is not as significant as that of the experimental method. The test method has achieved remarkable results in optimizing the running time of Delta robot sorting process. After optimization, the running time is 0.231 s, which is 6.60%

lower than that before optimization, and improves the working efficiency and overall performance of the robot.

The test method significantly reduces the average impact of each joint of the driving arm, and the impact decreases by 80.00%. Reducing joint impact helps improve the operational efficiency of the robot while extending the life of the robot.

In Table 8 and Figure 14, under the condition of resisting the load disturbance of branch a, the decoupling control effect of ESO combined with sliding mode is superior to that of average current decoupling control. It can be seen that the decoupling control strategy of ESO combined with sliding mode can effectively realize the decoupling between output branches, suppress the cross influence of branch A on branch B, and improve the response speed and anti-load disturbance ability of branch A

In the actual test, under the average current decoupling control, the voltage overshoot of branch B caused by load disturbance is 2 V, and the system recovers to steady state after about 16 ms. The voltage overshoot of branch a caused by the cross influence of branch B is 4 V, and the system recovers to steady state after about 14 ms; Under ESO combined with sliding mode decoupling control, the voltage overshoot of branch B caused by load disturbance is 1.5 V, and the rated voltage overshoot of branch a caused by the cross influence of branch B is 2 V. The system recovers to steady state after 6.3 ms.

In Table 10, the implementation scheme of neural approximator enhanced SMC can reduce the output voltage by 62% (from 1.2 V to 0.45 V) when the load step changes, while suppressing high-frequency chattering phenomenon (reducing the amplitude of switch frequency ripple by 40%), significantly improving the dynamic response quality.

In Table 11, through analysis of the experimental data, it can be seen that load changes and speed disturbances have a significant impact on motor tracking errors. The RMS error of the benchmark group is the lowest, while the error increase of the load mutation group reaches 128%, indicating that the randomness of the load has the greatest impact on system stability. The motion disturbance group mainly causes 8.3 Hz intermediate frequency oscillation, reflecting the response delay of the control loop; The composite disturbance group exhibits dual peak spectra of 18.6 Hz and 35.2 Hz simultaneously, confirming that the coupling effect between load and motion parameters exacerbates high-frequency vibrations. The data shows that load fluctuations are the dominant factor in errors, it is recommended to prioritize optimizing anti-interference algorithms in load mutation scenarios.

In a word, the decoupling control strategy based on extended state observer and sliding mode can effectively realize the decoupling between output branches, suppress the cross influence of branch B on branch a, and improve the anti-load disturbance ability of branch B. The above analysis verifies the global feasibility, indicating that the

stability analysis aims to eliminate the influence of cross coupling effect and disturbance on the global dynamics, rather than only improve the local performance.

When dealing with actuator saturation and joint/motor limitations in robot motion control, the core solution is to dynamically adjust the control output through ST-ESO real-time observation of system disturbances and load states. The anti-saturation compensation algorithm is used to handle torque limitations, and the joint position limit is avoided through a penalty function. Based on the estimated inertia of the observer, the acceleration is dynamically constrained, and finally a hierarchical constraint management system "position>velocity>torque>accuracy" is constructed to maximize motion performance while ensuring safety.

The industrial robot anti-interference control system compensates for communication delays through the ST-ESO state predictor (50 ms threshold switching local control), uses multi-source sensor fusion and Kalman filtering to achieve 200 ms fault tolerance, and establishes mechanism three-level interference response (mechanical collision/power fluctuation/communication interference corresponding to 100 ms/50 ms/200 ms recovery respectively). Moreover, it is integrated with the OPC UA protocol through the edge computing architecture (1ms control cycle).

The Simulink control model, C++core algorithm source code, and 750 experimental datasets (including complete sensor data under normal/interference conditions) of the system have undergone standardized desensitization processing, and all industrial sensitive parameters have been replaced with universal reference values. The model adopts modular design and has a certain degree of replicability

Through dynamic gain design, the bandwidth of the observer is automatically adjusted according to the motion state, targeting the internal force coupling disturbance unique to parallel mechanisms. Combined with a parameter self-tuning architecture based on Lyapunov exponent, the accuracy of the end effector trajectory is effectively improved. Compared with existing solutions, its originality lies in the integration of gain adaptation, parallel mechanism disturbance decoupling, and stability constraint parameter tuning, breaking through the bottleneck of accuracy and robustness of traditional ESO in high-speed parallel robots.

To further improve the ability of super-twisting sliding mode extended state observer to observe the total disturbance of inner and outer loops of CI-SIDOBuck converter, strengthen the ability of inner and outer loop controllers to compensate the total disturbance, and solve the problem that the parameter design of super-twisting ESO and super-twisting sliding mode control algorithms needs disturbance boundary information, firstly, a hyperbolic function is first used to replace the sign function in the super-twisting sliding mode extended state observer to further reduce system jitter, and a variable gain function that can change in real time with the observation error is designed to replace the linear gain of ST-ESO, thereby improving the observation capability of disturbances. Then, the generalized super-twisting sliding mode algorithm with linear terms is introduced as the approach law of the system, which smooths the control law of the system. Finally, the experimental verification shows that the sliding mode decoupling control strategy based on variable gain super-twisting ESO further improves the anti-disturbance ability and convergence speed of the system, and improves the overall performance of the system.

5 Conclusion

Based on the extended state observer commonly used in the field of strongly coupled systems such as motors and drones, this paper improves the super-twisting ESO and super-twisting sliding mode control algorithms by combining the control idea of decoupling with nonlinear control, and proposes an improved sliding mode decoupling control strategy for variable gain super-twisting ESO. Firstly, a hyperbolic function is used to replace the sign function in the super-twisting sliding mode extended state observer to further reduce system jitter, and a variable gain function that can change in real time with the observation error is designed to replace the linear gain of ST-ESO, thereby improving the observation capability of disturbances. Then, the generalized super-twisting sliding mode algorithm with linear terms is introduced as the approach law of the system, which smooths the control law of the system. Finally, the experimental research verifies that the practical effect of the model is obvious. Restrictive tests show that the proposed method further improves the ability of resisting input voltage disturbance, and improves the robustness and dynamic performance of the system.

However, the parameter design of the converter and the coupled single inductor multiple output converter are not discussed. Therefore, further research is needed to further demonstrate the application value of sliding mode decoupling control based on super-twisting extended state observer in such converters.

References

- [1] Almanza, C., Baquero, J. M., & Jiménez-Moreno, R. (2021). Robotic hex-nut sorting system with deep learning. International Journal of Electrical and Computer Engineering (IJECE), 11(4), 3575-3583. http://doi.org/10.11591/ijece.v11i4.pp3575-3583
- [2] Azar, A. T., Abed, A. M., Abdul-Majeed, F. A., Hameed, I. A., Jawad, A. J. M., Abdul-Adheem, W. R., Ibraheem, I. K., & Kamal, N. A. (2023). Design and stability analysis of sliding mode controller for non-holonomic differential drive mobile robots. Machines, 11(4), 470. https://doi.org/10.3390/machines11040470

- [3] Boysen, N., Schwerdfeger, S., & Ulmer, M. W. (2023). Robotized sorting systems: Large-scale scheduling under real-time conditions with limited lookahead. European Journal of Operational Research, 310(2), 582-596. https://doi.org/10.1016/j.ejor.2023.03.037
- [4] Briot, S., & Boyer, F. (2022). A geometrically exact assumed strain modes approach for the geometrico-and kinemato-static modelings of continuum parallel robots. IEEE Transactions on Robotics, 39(2), 1527-1543. https://doi.org/10.1109/TRO.2022.3219777
- [5] Cong, V. D. (2023). Visual servoing control of 4-DOF palletizing robotic arm for vision-based sorting robot system. International Journal on Interactive Design and Manufacturing (IJIDeM), 17(2), 717-728. https://doi.org/10.1007/s12008-022-01077-8
- [6] Dong, M., Zhou, Y., Li, J., Rong, X., Fan, W., Zhou, X., & Kong, Y. (2021). State of the art in parallel ankle rehabilitation robot: a systematic review. Journal of NeuroEngineering and Rehabilitation, 18(1), 52. https://doi.org/10.1186/s12984-021-00845-z
- [7] Duan, X., He, R., Zhao, Q., Chen, X., & Li, C. (2025). Unified admittance control for accurate puncture and respiration following based on disturbance observation and model predictive control. IEEE Robotics and Automation Letters, 10(4), 3526-3533. https://doi.org/10.1109/LRA.2025.3543145
- [8] Engelen, B., De Marelle, D., Diaz-Romero, D. J., Van den Eynde, S., Zaplana, I., Peeters, J. R., & Kellens, K. (2022). Techno-economic assessment of robotic sorting of aluminium scrap. Procedia CIRP, 105(2), 152-157.
 - https://doi.org/10.1016/j.procir.2022.02.026
- [9] Hassan, G., Gouttefarde, M., Chemori, A., Hervé, P. E., El Rafei, M., Francis, C., & Sallé, D. (2022). Time-optimal pick-and-throw S-curve trajectories for fast parallel robots. IEEE/ASME Transactions on Mechatronics, 27(6), 4707-4717. https://doi.org/10.1109/TMECH.2022.3164247
- [10] Hosseini-Pishrobat, M., & Keighobadi, J. (2019). Extended state observer-based robust non-linear integral dynamic surface control for triaxial MEMS gyroscope. Robotica, 37(3), 481-501. https://doi.org/10.1017/S0263574718001133
- [11] Jia, H.W., & Lianguang Mo, L.G. (2023). Study on water supply and drainage line layout method of large green building based on time series prediction. International Journal of Environmental Engineering, 12(2), 146-158. https://doi.org/10.1504/IJEE.2023.132634
- [12] Kiyokawa, T., Katayama, H., Tatsuta, Y., Takamatsu, J., & Ogasawara, T. (2021). Robotic waste sorter with agile manipulation and quickly trainable detector. IEEE Access, 9(2), 124616-124631. http://dx.doi.org/10.1109/ACCESS.2021.3110795
- [13] Kiyokawa, T., Takamatsu, J., & Koyanaka, S. (2022). Challenges for future robotic sorters of mixed

- industrial waste: A survey. IEEE Transactions on Automation Science and Engineering, 21(1), 1023-1040.
- https://doi.org/10.1109/TASE.2022.3221969
- [14] Konstantinidis, F. K., Sifnaios, S., Tsimiklis, G., Mouroutsos, S. G., Amditis, A., & Gasteratos, A. (2023). Multi-sensor cyber-physical sorting system (cpss) based on industry 4.0 principles: A multi-functional approach. Procedia Computer Science, 217(2), 227-237. https://doi.org/10.1016/j.procs.2022.12.218
- [15] Koskinopoulou, M., Raptopoulos, F., Papadopoulos, G., Mavrakis, N., & Maniadakis, M. (2021). Robotic waste sorting technology: Toward a vision-based categorization system for the industrial robotic separation of recyclable waste. IEEE Robotics & Automation Magazine, 28(2), 50-60. https://doi.org/10.1109/MRA.2021.3066040
- [16] Leveziel, M., Laurent, G. J., Haouas, W., Gauthier, M., & Dahmouche, R. (2022). A 4-DoF parallel robot with a built-in gripper for waste sorting. IEEE Robotics and Automation Letters, 7(4), 9834-9841. https://doi.org/10.1109/LRA.2022.3192582
- [17] Ma, H., Wei, X., Wang, P., Zhang, Y., Cao, X., & Zhou, W. (2022). Multi-arm global cooperative coal gangue sorting method based on improved Hungarian algorithm. Sensors, 22(20), 7987. https://doi.org/10.3390/s22207987
- [18] Moghanni-Bavil-Olyaei, M. R., Keighobadi, J., Ghanbari, A., & Olegovna Zekiy, A. (2023). Passivity-based hierarchical sliding mode control/observer of underactuated mechanical systems. Journal of Vibration and Control, 29(13-14), 3096-3111.
 - https://doi.org/10.1177/10775463221091035
- [19] Rushton, M., & Khajepour, A. (2022). An atlas-based approach to planar variable-structure cable-driven parallel robot configuration-space representation. IEEE Transactions on Robotics, 39(2), 1594-1606. https://doi.org/10.1109/TRO.2022.3218996
- [20] Satav, A. G., Kubade, S., Amrutkar, C., Arya, G., & Pawar, A. (2023). A state-of-the-art review on robotics in waste sorting: scope and challenges. International Journal on Interactive Design and Manufacturing (IJIDeM), 17(6), 2789-2806. https://doi.org/10.1007/s12008-023-01320-w
- [21] Shang, D., Zhang, L., Niu, Y., & Fan, X. (2022). Design and key technology analysis of coal-gangue sorting robot. Coal Science and Technology, 50(3), 232-238.
 - http://dx.doi.org/10.13199/j.cnki.cst.ZN20-040
- [22] Sun, Z., Huang, L., & Jia, R. (2021). Coal and gangue separating robot system based on computer vision. Sensors, 21(4), 1349. https://doi.org/10.3390/s21041349
- [23] Wang, Y., An, T., Cui, Y., Li, Y., & Dong, B. (2024).

 Decentralized position/torque control of modular robot manipulators via interaction torque estimation-based human motion intention identification. International Journal of Control,

- Automation and Systems, 22(5), 1585-1600. https://doi.org/10.1007/s12555-023-0004-8
- [24] Wu, P., Wang, Z., Jing, H., & Zhao, P. (2022). Optimal time-jerk trajectory planning for delta parallel robot based on improved butterfly optimization algorithm. Applied Sciences, 12(16), 8145. https://doi.org/10.3390/app12168145
- [25] Zhang, H., Liang, H., Ni, T., Huang, L., & Yang, J. (2021). Research on multi-object sorting system based on deep learning. Sensors, 21(18), 6238. https://doi.org/10.3390/s21186238